Article

Transiently Thermoresponsive Acetal Polymers for Safe and Effective Administration of Amphotericin B as Vaccine Adjuvant

Simon Van Herck, Lien Van Hoecke, Benoit Louage, Lien Lybaert, Ruben De Coen, Sabah Kasmi, Aaron P Esser-Kahn, Sunil A. David, Lutz Nuhn, Bert Schepens, Xavier Saelens, and Bruno G. De Geest

Bioconjugate Chem., **Just Accepted Manuscript** • DOI: 10.1021/acs.bioconjchem.7b00641 • Publication Date (Web): 26 Nov 2017

Transiently Thermoresponsive Acetal Polymers for Safe and Effective Administration of Amphotericin B as Vaccine Adjuvant

Simon Van Herck,[†,‡] Lien Van Hoecke,[§,∥] Benoit Louage,[†,‡] Lien Lybaert,[†,‡] Ruben De Coen,[†,‡] Sabah Kasmi,[†,‡] Aaron P. Esser-Kahn,[⊥] Sunil A. David,[#] Lutz Nuhn,[†,‡] Bert Schepens,[§,∥] Xavier Saelens,[§,∥] Bruno G. De Geest*[,†,‡]

[†]*Department of Pharmaceutics, Ghent University, Ottergemsesteenweg 460, 9000 Ghent, Belgium*

[‡]*Cancer Research Institute Ghent (CRIG), Ghent University, Belgium*

[§]*VIB-UGent Center for Medical Biotechnology, Technologiepark 927, 9052 Ghent, Belgium*

[∥] *Department of Biomedical Molecular Biology, Ghent University, Ghent B-9052, Belgium.*

[⊥]*Department of Chemistry, University of California, Irvine, Irvine, California 92697, United States*

[#]*Department of Medicinal Chemistry, University of Minnesota, Sixth Street SE, Minneapolis, Minnesota 55455, United States.*

Corresponding author: br.degeest@ugent.be

ABSTRACT: The quest for new potent and safe adjuvants to skew and boost the immune response of vaccines against intracellular pathogens and cancer has led to the discovery of a series of small molecules that can activate Toll like receptors (TLRs). Whereas many small molecule TLR agonists cope with a problematic safety profile, Amphotericin B (AmpB) – an FDA-approved anti-fungal drug – has recently been discovered to possess TLR triggering activity. However, its poor aqueous solubility and cytotoxicity at elevated concentrations currently hampers its development as a vaccine adjuvant. We present a new class of transiently thermoresponsive polymers that in native state have a phase transition temperature below room temperature, but gradually transform into fully soluble polymers through acetal hydrolysis at endosomal pH values. RAFT polymerization afforded well defined block copolymers that self-assemble into micellar nanoparticles and efficiently encapsulate AmpB. Importantly, nanoencapsulation strongly reduced the cytotoxic effect of AmpB, but maintained its TLR triggering capacity. Studies in mice showed that AmpB loaded nanoparticles can adjuvant an RSV vaccine candidate with almost equal potency as a highly immunogenic oil-in-water benchmark adjuvant.

INTRODUCTION

The traditional vaccination paradigm relying on weakened or killed version of pathogens is failing for a wide number of viruses (e.g. HIV, RSV) and bacteria (e.g. mTB) as well as for therapeutic anti-cancer vaccination.[1] Therefore, novel strategies are endeavored based on subunit proteins and peptides to direct the immune response against more conserved epitope domains or epitopes that are not involved in immune escape mechanisms.[2] Furthermore, adjuvants have become essential components in many vaccines to modulate the interaction between antigen presenting cells, T cells and B cells, thereby skewing and amplifying the adaptive immune response.[3] Several molecular adjuvants work by binding to pattern-recognition receptors (PRRs), like the Toll-like receptors (TLRs), leading to the secretion of immunostimulatory cytokines and type-I IFN.[4,5] Over the years promising results have been achieved for small molecule agonists, in particular for TLR 4, 7, 8 and 9.[6–12] Interestingly, a recent high content screening of 10^5 registered drug compounds by the David group has led to the identification of amphotericin B (AmpB) as activator of TLR 2 and 4.[13] Owing to its well established safety record and FDA approved status, AmpB would be suitable for vaccine formulation. However, AmpB is poorly water-soluble and needs either covalent modification to render it more water soluble or encapsulation in polymeric and liposomal formulations.[14–16] Despite its well established immunostimulatory properties[17] to our knowledge no attempts have been made in formulating AmpB with the focus on its use as a vaccine adjuvant.

With regard to the formulation of small molecule adjuvants there lies an important role for the delivery route to antigen presenting cells.[18,19] Whereas water soluble molecular adjuvants hold the risk of systemic inflammation, nanoparticulate carriers can strongly limit this risk by directing the activity of molecular adjuvants to the immune-inducing sites in the draining lymph nodes[20] as recently shown by our group[7] and others.[21,22] Despite its FDA-approved state, an important constraint of AmpB is it cytotoxic action within a concentration window that is relevant for adjuvant activity. Therefore, we sought for a strategy to formulate AmpB as nanoparticles under benign conditions to alleviate cytotoxicity but retain its adjuvanticity.

In this paper we develop a novel type of transiently thermoresponsive block copolymer[23] nanoparticles to formulate AmpB (**Scheme 1A**) in the hydrophobic nanoparticle cavity (**Scheme 1B**). Such polymers reversibly form nanoparticles starting from a cooled polymer solution followed by a mild temperature increase not higher than ambient conditions, but lose this property – i.e. become fully water-soluble irrespective of temperature – as consequence of an alteration of the polymer side chain or backbone triggered by a physiologically relevant stimulus.[23,24] The endosomal acidic pH of 5-5,5 is attractive to trigger such nanoparticle degradation and acetal/ketal chemistry has been used to serve this purpose. [25,26] Much research

is done on polyacetal/ketal synthesis by step-growth polymerization.[27–31] However, much less has been reported on acid-sensitive vinyl monomers that can be polymerized via controlled (radical) polymerization methods, with virtually no systems being reported which allow for degradation over an acceptably short timeframe within a physiologically relevant pH window.[26,32,33]

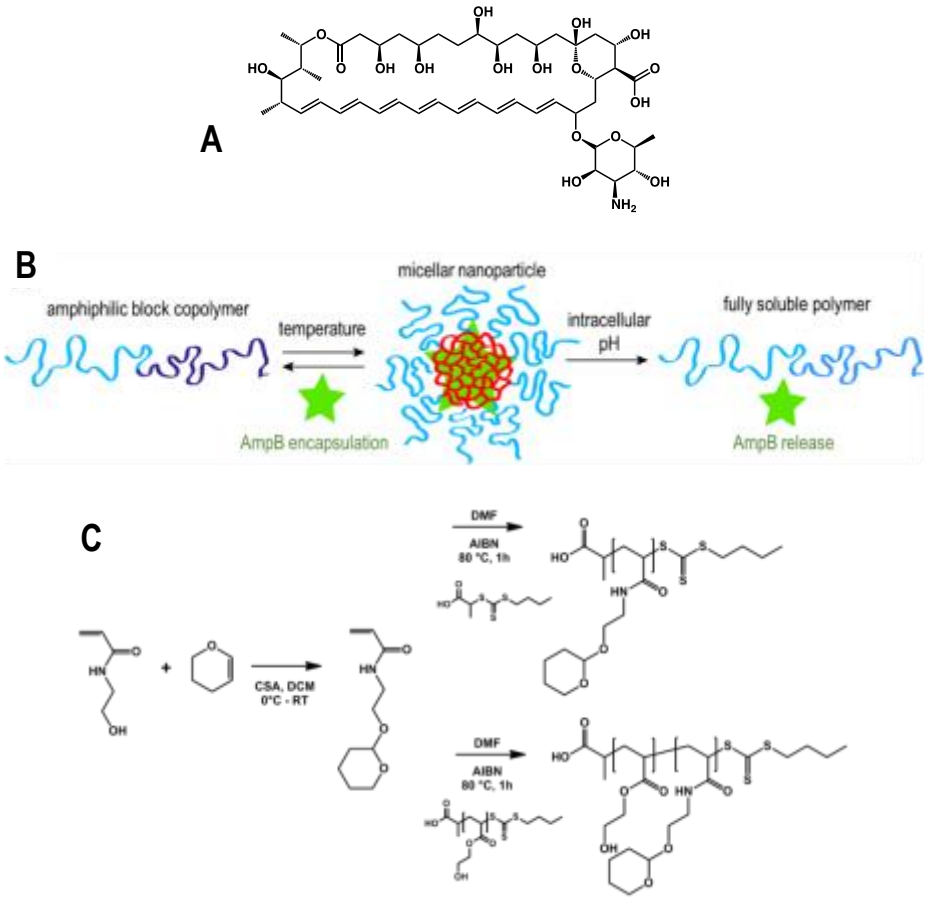

Scheme 1. (A) Molecular structure of Amphotericin B. **(B)** Schematic representation of AmpB encapsulation in acid-sensitive transiently thermoresponsive nanoparticles. **(C)** Synthesis and RAFT (block co) polymerization of HEAmTHP.

RESULTS AND DISCUSSION

We engineered the water-soluble acrylamide 2-hydroxyethylacrylamide (HEAm), a readily available hydrophilic monomer, with an acid-sensitive hydrophobic acetal moiety using 3,4-dihydro-2H-pyran (DHP), known from protecting group chemistry,[34] yielding N-[2-[(tetrahydro-2H-pyran-2-yl)oxy]ethyl]-acrylamide(HEAmTHP) (**Scheme 1C**). The applicability of the DHP group to form acid-degradable monomers through acetal linkage has been explored earlier by Klaikherd and co-workers[35] on methacrylates (i.e. 2-hydroxyethylmethacrylate (HEMA)), yielding acid-degradable, but fully hydrophobic, polymers. In our endeavors to design transiently responsive polymers, the use of acrylamides instead of (meth)acrylates, takes advantage of the presence of the amide moiety which gives the repeating units a more hydrophilic character, through hydrogen bonding with water molecules below the phase transition temperature (for the sake of simplicity denoted as Tcp, cloud point temperature, further in this paper) of the polymers. However, dehydration of the acrylamide side chains on its turn should provide a driving force for globule formation above a critical Tcp.[24,36,37]

Reactions were conducted at low temperature using equimolar amount of HEAm and DHP. Excess DHP resulted in lower yields due to formation of a side product, possibly formed by an “inverse demand” Diels-Alder reaction between the alkene of DHP and the vinyl group of HEAm. NMR spectra of the purified monomer are provided in (**Figure S1**). MS analysis and the proposed structure of the aforementioned side product are shown in **Figure S2**. Degradability of the monomer in acidic buffer at pH 5 was confirmed by ^{1}H-NMR analysis (**Figure 1A**) showing the shift of the acetal proton (**b**) to the lactol proton (**c**). The pH-dependent hydrolysis rate is evaluated in aqueous buffers at pH 5 and 7.4 representing lysosomal and physiological pH conditions, respectively, by HPLC analysis (**Figure 1B**). Whereas a half-life of less than 24h was observed at pH 5, minimal hydrolysis was observed at pH 7.4, even after extended periods of time.

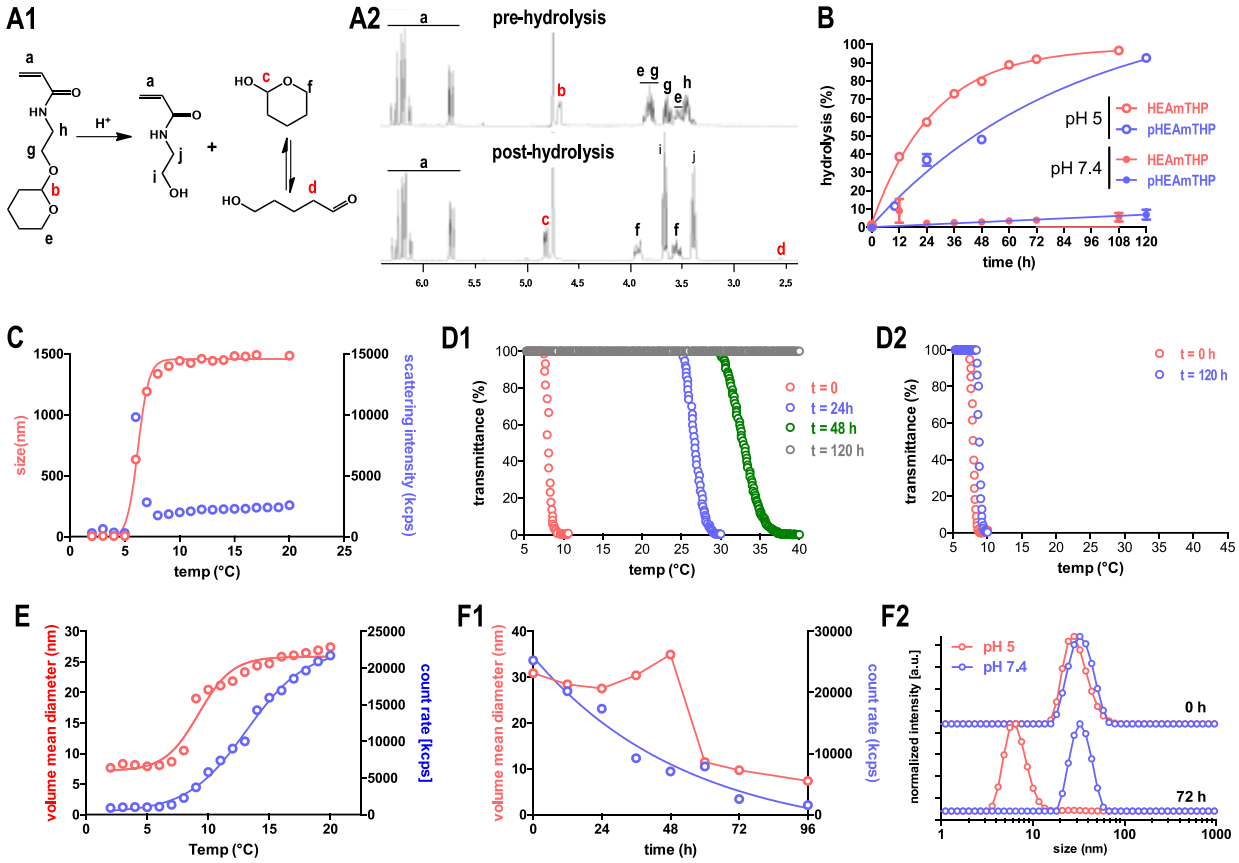

Figure 1. Reaction scheme **(A1)** and ^{1}H-NMR spectra **(A2)** of HEAmTHP before and after hydrolysis in deuterated buffer at pH 5. The most relevant H-peaks for hydrolysis are indicated in red. The peak annotated with "d" corresponds to the protons attached to the α-C of 5-hydroxypentanal which is only formed in very small amounts. **(B)** Degradation profiles in function of time of HEAmTHP and pHEAmTHP$_{42}$ (P01) at pH 5 and pH 7.4 analyzed by HPLC or NMR. **(C)** Mean particle diameter (red) and scattering intensity (blue) profiles in function of temperature analyzed by DLS at 5 mg/mL in PBS for pHEAmTHP$_{42}$ (P01). **(D)** Transmittance profiles of pHEAmTHP$_{42}$ (P01) dispersions in function of temperature at different time points during hydrolysis at pH 5 (**D1**) and pH 7.4 (**D2**) analysed by turbidimetry. **(E)** Temperature induced self-assembly of **P6** (**p(HEA$_{110}$-HEAmTHP$_{47}$)**) shown as average volume diameter (red) and scattering intensity (blue) in function of temperature measured by DLS in PBS. **(F)** pH dependent hydrolysis and disassembly of nanoparticles based on **P6**. Volume mean diameter (red) and scattering intensity (blue) as function of time at pH 5 (**F1**) and volume mean diameter (**F2**) at 2 different time points measured at pH 5 (red) and pH 7.4 (blue).

Homopolymers of HEAmTHP were synthesized by Reversible Addition-Fragmentation Chain Transfer (RAFT) polymerization using 2-(butylthiocarbonothioylthio)propionic acid (PABTC) as chain transfer agent (CTA), aiming at a degree of polymerization (DP) of 50 or 100 (**Table 1**). As an example, the ^{1}H NMR spectra of the purified polymers are shown in **Figure S4**. Based on ^{1}H NMR analysis of the monomer conversion a theoretical DP of 42, 66 was calculated for pHEAmTHP. For the sake of clarity, further on in this paper, the theoretical DP values will be mentioned in subscript when referring to a specific polymer. According to size

exclusion chromatography (SEC) analysis, narrowly dispersed polymers were obtained, with dispersity (Đ) values of 1.12 and a number average molecular weight (M_n) of 8,6 and 13,4 kDa for $pHEAmTHP_{42}$ (P01) and $pHEAmTHP_{66}$ (P02), respectively. (**Table 1**, **Figure S5**). The thermoresponsive properties of the polymers were measured by dynamic light scattering (DLS) (**Figure 1C and Figure S6**) at a polymer concentration of 5 mg/mL in phosphate buffered saline (PBS; pH 7.4, 0.15 M NaCl) and revealed a cloud point temperature T_{cp} well below room temperature. The transiently thermoresponsive behavior properties – i.e. a gradual shift in T_{cp} upon hydrolysis of the pending THP moieties - of the polymers was investigated by turbidimetry on a colloidal suspension of pHEAmTHP (P01 or P02) at 37 °C (**Figure 1D and Figure S7**). A clear shift in T_{cp} was found which proves that pHEAmTHP loses its hydrophobic properties to become fully soluble irrespective of temperature.

Table 1. Polymer composition and properties of the synthesized (block co)polymers.

No.		CTA	M:CTA		conversion (%)	DP[a]	M_n[a] (kDa)	M_n[b] (kDa)	Đ
			[HEA]	[HEAmTHP]					
P01	**$pHEAmTHP_{42}$**	PABTC		50:1	83.8	42	8.6	7.4	1.12
P02	**$pHEAmTHP_{66}$**	PABTC		100:1	66	66	13.4	12.1	1.12
P03	**$pHEA_{78}$**	PABTC	100:1		78	78	9.3	17.5	1.14
P04	**$pHEA_{110}$**	PABTC	150:1		73	110	13.0	21.9	1.17
P1	**$p(HEA_{78}$-$HEAmTHP_{19})$**	$pHEA_{78}$		21:1	93	19	13.1	21.5	1.16
P2	**$p(HEA_{78}$-$HEAmTHP_{38})$**	$pHEA_{78}$		40:1	94	38	16.9	23.0	1.16
P3	**$p(HEA_{78}$-$HEAmTHP_{53})$**	$pHEA_{78}$		60:1	88	53	19.9	25.1	1.16
P4	**$p(HEA_{78}$-$HEAmTHP_{70})$**	$pHEA_{78}$		83:1	85	70	23.2	26.9	1.14
P5	**$p(HEA_{110}$-$HEAmTHP_{26})$**	$pHEA_{110}$		30:1	87	26	18.6	27.3	1.17
P6	**$p(HEA_{110}$-$HEAmTHP_{47})$**	$pHEA_{110}$		54:1	87	47	22.4	29.8	1.15
P7	**$p(HEA_{110}$-$HEAmTHP_{70})$**	$pHEA_{110}$		85:1	82	70	27.0	30.9	1.17
P8	**$p(HEA_{110}$-$HEAmTHP_{87})$**	$pHEA_{110}$		116:1	75	87	30.3	35.4	1.15

[a]Calculated based on ^{1}H NMR spectroscopy data. [b]Determined by SEC in DMAc using PMMA for calibration.

Amphiphilic block copolymers containing pHEAmTHP as responsive block were synthesized by RAFT polymerization as shown in **Scheme 1**. For the hydrophilic segment, 2-hydroxyethylacrylate (HEA) was selected, using a pHEA macroCTA approach, as it was – at least in our hands – not possible to obtain block copolymers using pHEAm as macroCTA. Neither was it possible to chain extend pHEAmTHP with HEAm. We attribute this to incompatibility issues between the respective monomers and the solvent system used for RAFT polymerization. Similar issues were also encountered recently within our laboratories and could also

be resolved by combining acrylates with acrylamides.[38] A pHEA macroCTA was synthesized (**Figure S8** for ^{1}H NMR) with a targeted DP of 100 and 150, and the polymerization reaction was stopped before 80 % conversion to ensure good chain end fidelity. ^{1}H NMR analysis revealed a theoretical DP of 78 and 110, respectively. SEC analysis (**Figure S10**, red curves) confirmed the polymers to be narrowly dispersed, Đ of 1.14 and 1.17, with absence of tailing (**Table 1**). Next, the pHEA macroCTAs were used for the synthesis of a series of block copolymers (**Table 1, Figure S9 and S10**). The chain length of the hydrophobic block was varied to investigate its influence on the self-assembly behavior, temperature responsiveness, degradation rate and ability to encapsulate hydrophobic compounds. SEC analysis of these block copolymers revealed that all were obtained with a narrow dispersity, giving proof of well controlled block copolymerization (**Table 1 and Figure S10**).

The influence of the hydrophobic chain length and total chain length on the self-assembly behavior was investigated in aqueous medium. An overview of these results is given in **Table 2**. Interestingly, all pHEA-HEAmTHP block copolymers were able to self-assemble into small and defined micellar nanoparticles with low polydispersity and Z-average values ranging from 26 nm to 36 nm for polymers **P1-P4** and from 28 nm to 42 nm for polymers **P5-P8** at 37 °C in PBS. An increase in HEAmTHP chain length resulted in an increase in particle size (**Figure S11)**. The influence of temperature on the self-assembly behavior of the block copolymers was measured by DLS (**Figure 1E**) where a strong influence of the polymer chain length on the phase transition temperature was observed, with shorter polymer chain lengths yielding a higher Tcp value. The critical association concentration (CAC) was determined via pyrene assay and also indicated a strong influence of the HEAmTHP content. Overall, a compelling correlation was seen between the hydrophobic chain length and the hydrodynamic diameter, the Tcp and CAC (**Table 2, Figure S11**), with decrease in CAC and Tcp upon increasing hydrophobic content. The latter, together with the ease of particle formation that proceeds via mere dissolution of the block copolymers in cold (i.e. below the Tcp) PBS followed by heating to room temperature, makes the HEA-HEAmTHP polymer combination an appealing system for drug formulation. The effect of the pH dependent acetal hydrolysis on the nanoparticle stability was investigated by DLS at pH values of 7.4 and 5. As shown in **Figure 1F**, the nanoparticles are stable at pH 7,4, but gradually disassemble in acidic medium (**Figure 1F1**), finally resulting in soluble unimers (**Figure 1F2**).

Table 2. Overview of the supramolecular properties of synthesized pHEA$_x$-HEAmTHP$_y$ block copolymers.

	H_2O		PBS						T_{cp} (°C)[1]	CAC (µg/mL)[2]
	25°C		5°C		25°C		37°C			
	Z-average (nm)	PdI	Z-average (nm)	PdI	Z-average (nm)	PdI	Z-average (nm)	PdI		
P1	12.7 ±0.3	0.19	5.8 ±0.4	0.63	19.9 ±0.1	0.11	26.3 ±0.6	0.24	22	38,2
P2	14.1 ±0.3	0.21	7.4 ±0.7	0.53	27.5 ±0.3	0.05	29.2 ±0.5	0.03	10	23,0
P3	13.0 ±0.3	0.18	7.8 ±0.2	0.50	35.7 ±0.2	0.04	35.4 ±0.1	0.04	8	10,4
P4	29.4 ±4.9	0.40	7.8 ±0.3	0.31	41.3 ±1.1	0.06	36.1 ±1.6	0.06	5	8,47
P5	14.0 ±0.4	0.36	7.5 ±0.6	0.64	25.9 ±0.4	0.10	27.9 ±0.1	0.08	13	40,2
P6	14.2 ±0.2	0.20	7.9 ±0.3	0.72	32.0 ±0.1	0.07	32.5 ±0.1	0.02	9	16,9
P7	12.5 ±0.2	0.09	7.9 ±0.4	0.62	35.5 ±0.3	0.05	36.3 ±0.04	0.03	8	8,71
P8	18.3 ±0.3	0.18	47.5 ±11	0.33	54.8 ±0.8	0.13	42.4 ±0.3	0.01	5	5,53

[1] Measured in PBS at 5 mg/mL; [2] Dilutions made in 0.1 M phosphate buffer, measurement done in triplicate

Next, we aimed at investigating the potential of our transiently responsive polymer system as a nanoscopic delivery system in a biomedical context. Initially, we assessed whether the block copolymer micelles could entrap a hydrophobic payload and deliver this to dendritic cells (DCs). DCs, as the most potent antigen presenting cells, are the prime target in the scope of formulating an adjuvant nanocarrier.[5,19] In first instance we made use of the hydrophobic fluorescent dye, 1,4-bis[1-cyano-2-(diphenylamino)phenyl)vinyl]benzene (DSB),[39] as a model compound for physical encapsulation in order to visualize intracellular uptake. Encapsulation of DSB in pHEA$_x$-HEAmTHP$_y$ nanoparticles was accomplished by solvent diffusion from acetone into PBS. Quantification of the amount of encapsulated DSB was done by UV-Vis spectroscopy after filtration to remove non-encapsulated precipitated dye and freeze drying (**Figure S12**). Control experiments were performed in only PBS without block copolymer while using **P03** without polyHEAmTHP segment as a hydrophilic-only control. All pHEA-HEAmTHP block copolymers were able to encapsulate the hydrophobic DSB to a similar extent. Also, merely hydrophilic pHEA homopolymer could stabilize DSB, albeit to a much lesser extent. From these results, **P6** was chosen to assess whether these block copolymers could increase the intracellular delivery of the hydrophobic DSB. For this purpose, DC2.4 (an immortalized mouse dendritic cell line) cells were pulsed with DSB formulated either in **P6** nanoparticles or in **P03** as a control. Subsequently, confocal microscopy was used to monitor the intracellular fate of the DSB. From **Figure 2A**, it is clear that DSB formulated with **P6** leads to a punctuated intracellular fluorescence pattern (green dots), whereas no uptake of DSB could be observed in cells pulsed with DSB admixed with polyHEA. Note that both images were recorded and processed using identical settings.

Encouraged by the observed superiority of **P6** nanoparticle system in effectuating the intracellular uptake of a hydrophobic compound by DCs in comparison to free component, we use this block copolymer for the formulation of AmpB, which was the primary target compound in our study. In a first series of experiments, we screened different conditions to formulate AmpB using **P6**. Due to the limited solubility of AmpB in most organic solvents,[14] solvent diffusion from DMSO into PBS was selected. We initially selected diluting a DMSO solution with PBS. Variations were made in the concentration of AmpB and polymer (**P6**), and in AmpB to polymer ratio (i.e. 1:10, 1:2 or 1:1). A graphical overview of these results can be found in **Figure S15**. Quantification of the encapsulated AmpB content was done by UV-Vis spectroscopy. For the latter, formulations were diluted with DMSO to release AmpB from the micelles, which yielded a typical multi-peak absorbance spectrum of AmpB shown in **Figure S13**. Encapsulation efficiency was found to increase with increasing polymer concentration. At lower polymer concentrations (1 mg/mL and 5 mg/mL) the 1:2 AmpB:polymer ratio yielded the best results regarding absolute encapsulated AmpB amount. This was however not the case for polymer concentrations at 10 mg/mL, as the 1:10 ratio proved to be most efficient. In this respect, the 1:10 ratio and a polymer concentration of 10 mg/mL was selected for further experiments based on the good encapsulation efficiency and absolute encapsulated concentration. Control experiments were performed in a similar fashion without block copolymer or only hydrophilic pHEA. In those cases, no AmpB was detected by UV-VIS after filtration indicating that amphiphilic block copolymers were necessary to efficiently solubilize AmpB. The above-elucidated optimal formulation conditions were used to evaluate the influence of hydrophobic chain length and total chain length of $pHEA_x$-$HEAmTHP_y$ block copolymers on AmpB loading efficiency. Comparable results were obtained for encapsulation efficiency ranging between 35 % and 50 % (**Figure S16**), indicating that all polymers are suitable to prepare formulations. Overall, both **P2** and **P6** were found to be most suitable for formulating AmpB based on the polymer properties and encapsulation efficiency. The formulation method was further optimalized and scaled-up for **P6**. Finally up to 95 % of AmpB encapsulation was achieved by dropwise addition of a concentrated AmpB solution in DMSO into the polymer dispersion under vigorous stirring. The formulations were dialysed to remove the DMSO and freeze dried to have it in dry powderish form which could easily be redispersed in PBS to give a stable AmpB-NP formulation (**Figure S17**).

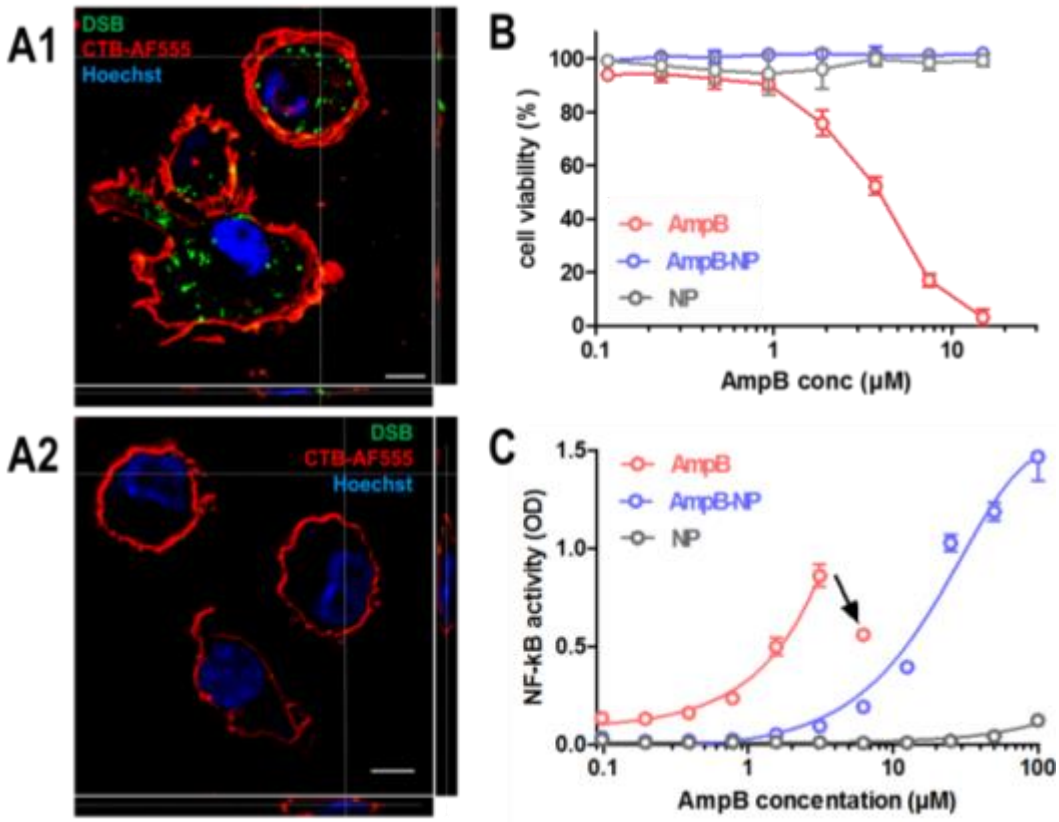

Figure 2. (A) Confocal microscopy images of DCs pulsed at 37°C with DSB (green channel) formulated with **P6** (**A1**) or **P03** (**A2**). Cell membrane staining was done with AlexaFluor555 conjugated cholera toxin B (red channel) and cell nuclei staining was done with Hoechst (blue channel). Images are confocal xy section with the corresponding orthogonal xz and yz planes. Identical settings for excitation power, detection sensitivity and contrast were used for recording. Scale bar represents 10 µm. **(B)** *In vitro* cytotoxicity of AmpB-NP(**P6**), free AmpB and unloaded polymer (**P6**) on murine RAW 264.7 macrophages after 24h incubation. The graph shows the cell viability as measured by MTT assay. Cell viability of PBS treated cells was set as 100%. (n=6, mean + SD). **(C)** NF-κB induction in RAWBlue cells pulsed with a concentration range of AmpB, AmpB-NP (**P6**), and empty NP (**P6**) control. NF-κB activity presented relative to secreted embryonic alkaline phosphatase (SEAP) production detected by QUANTI-Blue assay. Note that these experiments were performed with nanoparticles (NP) composed of **P6** (n=6, mean + SD). The black arrow highlights the drop in activity that is due to cytotoxicity.

To evaluate the adjuvant properties of AmpB loaded nanoparticles we firstly evaluated the *in vitro* cytotoxicity of our formulations in a murine RAW 264.7 macrophage cell line. The MTT assay indicated (**Figure 2B**) no cytotoxicity for both the polymer and the AmpB formulations over a concentration range from 0.1 – 30 µM. By contrast, AmpB in soluble form, i.e. diluted from DMSO in cell culture medium, was (highly) toxic with an LC50 value at approximately 4 µM. Note that this effect was not due to the presence of the minimal amount of DMSO used to primarily dissolve the AmpB, as a control experiment comprising only DMSO did not show

any cytotoxicity. Moreover, the cytotoxic effect of AmpB as such has been reported earlier by others as well.[40,41] Interestingly, AmpB formulated in **P6** did not cause any cytotoxicity, at least not within the operated experimental window. The most commonly accepted mechanism of action and toxicity involves the formation of ion channels[40,42,43] and is related to the physical state of the drug.[14,44,45] It has been reported by various researchers that at low AmpB concentrations, where AmpB is in its monomeric form, it is less toxic towards mammalian cells. In contrast, above certain concentrations, when self-associated AmpB species form, it is nonselective and evokes cell lysis in both mammalian and fungal cells.[14,15,44] However, binding conclusions cannot be drawn from earlier reports studying this link due to presence of toxic solvents or surfactants in their experiments.[14,45] The non-toxic behavior of the AmpB loaded nanoparticles could imply that the pHEA-HEAmTHP block copolymers stabilize the AmpB in its monomeric form, thus making it non-toxic towards murine macrophages.

Second, we tested the ability of the formulations to induce TLR activation using the RAW-Blue reporter cell line. These are murine derived RAW 264.7 macrophages that secrete an alkaline phosphatase (SEAP) upon activation of NF-κB, e.g. after TLR stimulation. A comparison is made between free AmpB and AmpB loaded micelles of block copolymer **P6**. Empty micelles were included as a control. NF-κB activity is presented as an increase in optical density, measured at 620 nm, relative to the negative control. The results in **Figure 2C** indicate that **P6** based AmpB formulations can activate NF-κB. The absence of stimulation when only polymer is present shows that the activity is linked to AmpB released from the nanoparticle and not to the polymer. Free AmpB in its soluble monomeric form is at low concentration, below 1 μM, more potent in TLR activation than in micelle-encapsulated form. However, at concentrations above 1 μM, TLR activation of the soluble AmpB drops. Most likely this drop results from the detrimental effect of free AmpB on cell viability at concentrations above 1 uM (**Figure 2B**). The underlying reason for the reduced TLR agonistic activity of AmpB loaded NP in comparison with free AmpB is likely a more efficient triggering of the cell membrane bound TRL2/4 in soluble form than in micelle-encapsulated form.[5,46] However, more importantly, micelle-encapsulation allows for the use of higher AmpB concentrations, reaching overall a more potent TLR triggering (as the measured OD values of micelle-encapsulated kept on increasing above the value reached at 1 μM of soluble AmpB) while avoiding toxicity issues.

Encouraged by these findings, the final aim of this study was to evaluate the potential of AmpB loaded nanoparticles as a vaccine adjuvant *in vivo*. To this end we prepared vaccine formulations by admixing nanoparticles based on **P6** with an antigen derived from human respiratory syncytial virus (RSV). RSV is one of the leading causes of airway infections worldwide and is the leading cause of infant hospitalization.[48]

Although in most cases RSV causes mild upper respiratory tract infections, the virus can also spread the lower respiratory tract, which, in infants, can lead to bronchitis and increased risk of recurrent wheezing and allergic asthma at a later age.[49] The inability of natural RSV infection to elicit protective immunity and the observation that individuals with RSV-neutralizing antibodies in their serum can be reinfected with RSV has hampered vaccine development. One RSV vaccine candidate, which is currently evaluated in a phase I trial, is based on the extracellular part of the small hydrophobic protein (SHe) of RSV.[50] Interestingly, the mechanism of action of SHe-based vaccination does not rely on neutralizing antibodies but rather on binding of anti-SHe antibodies to the surface of infected cells and subsequent induction of antibody-mediated cell killing or phagocytosis. SHe is naturally poorly immunogenic and to explore its potential as a protective vaccine antigen, the immunogenicity of SHe has to be boosted. In our present study, we made use of a SHe-KLH (KLH: keyhole limpet hemocyanin) fusion protein that was previously reported to elicit SHe-specific antibodies that can control RSV replication in a mouse model.[50] DLS analysis showed no influence of the presence of the SHe-KLH protein on the colloidal stability of the nanoparticles (**Figure S19**).

As well established adjuvant formulation, we opted for Sigma Adjuvant System (SAS), which is a commercially available oil-in-water emulsion based on squalene as oil phase stabilized with Tween80 as surfactant. Furthermore, it contains monophosphoryl lipid a (MPLA) from *Salmonella minnesota* and synthetic Trehalose dicorynomycolate (TDM). SAS is therefore comparable to the Ribi adjuvant and Freund's adjuvant system, and often used for preclinical models, *e.g*. to assess the potency of new adjuvant systems against a very competitive benchmark. In our present experiments formulations were prepared by admixing KLH conjugated SHe-antigen with the respective adjuvants systems. She-KLH antigen only, antigen admixed with empty (i.e. non-AmpB loaded) nanoparticles and a PBS were included as controls. Note that it was impossible to prepare an antigen + free AmpB formulation due to the inability of AmpB to dissolve in aqueous medium at the required concentration for immunization. Cohorts of 5 BALB/c mice per group were immunized subcutaneously with one prime and one boost injection. Total anti-RSV SHe IgG antibody titers in serum were determined pre- and post-immunization and the dilution curves measured by a SHe-peptide based ELISA (enzyme linked immunosorbent assay) are depicted in **Figure 3A-B**. In addition, the end point titers are shown in **Figure 3C**. From these data, it is clear that antigen only and antigen formulated with empty nanoparticles are poorly immunogenic and only raise detectable antibody titers after the boost immunization. These findings also point out the low immunogenicity of the nanoparticles themselves. By contrast, antigen adjuvanted with SAS or AmpB-loaded nanoparticles induce robust antibody responses from the prime immunization onwards that are further increased upon the booster immunization. No significant differences

in SHe-specific antibody titers were observed between SAS and AmpB-loaded nanoparticles. This underscores the potency of the newly developed AmpB-loaded nanoparticles which does not involve bacteria cell wall components and are based on AmpB, an established and FDA approved drug molecule. To investigate whether the deployed immunization strategy could counteract RSV infection, mice were challenged with 10^6 plaque-forming units (PFU) of HRSV A2 followed by dissection of the lungs 5 days post-infection and measuring viral lung titers in an *in vitro* plaque formation assay.[50] As depicted in **Figure 3C**, immunization with antigen adjuvanted with either SAS or AmpB-loaded nanoparticles significantly lowered RSV replication in the lung, again pointing out the excellent performance of our presently reported adjuvant system compared to a potent benchmark adjuvant.

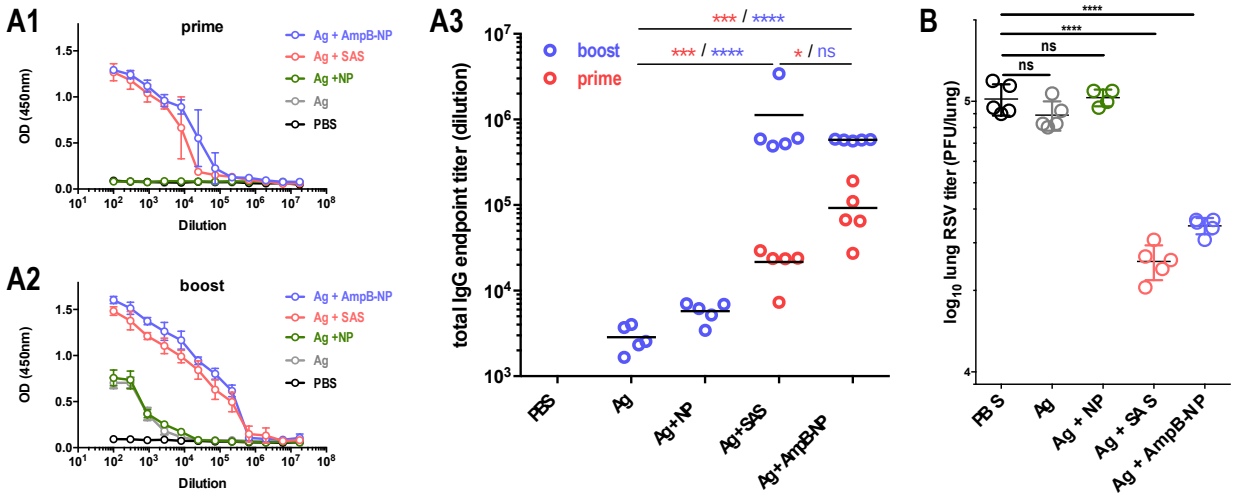

Figure 3. Serum dilution curves after (A1) prime and (A2) boost immunization and (A3) end-point titers tested in a SHe peptide ELISA assay. (n=5) (B) Number of plaque forming units (PFU) in the lungs of immunized mice that had been challenged with RSV. (n=5) (*<0,0001; student t-test against PBS group). The results shown are from a single *in vivo* experiment.

CONCLUSIONS

Summarizing, a novel non-toxic acid-degradable, transiently thermoresponsive block copolymer system was synthesized based on the modification of the hydrophilic 2-hydroxyethyl acrylamide (HEAm) with tetrahydropyran via degradable acetal bonds. Controlled polymerization by RAFT resulted in well-defined block copolymers. Degradation studies showed that the acetal moiety of the monomers and the polymers made thereof were prone to hydrolysis under acidic conditions in a relevant pH and time framework, but remained intact at physiological pH. All pHEA-HEAmTHP block copolymers formed small, 20-40 nm, micellar structures in PBS and degraded fast to fully soluble polymer at acidic pH. A strong correlation was observed between the hydrophobic chain and the temperature responsiveness and the CAC.

The nanoparticle system was shown to be very efficient in solubilizing hydrophobic compounds and enhancing their intracellular delivery. Importantly, nanoparticle formulation abrogated the cytotoxicity of Amphotericin B, while retaining it immunomodulatory properties as a TLR agonist. *In vivo* immunization experiments in mice using a poorly immunogenic SHe-KLH fusion protein as a newly found promising RSV antigen showed the induction of robust antibody response and reduction of viral lung titers to the same extent as antigen adjuvanted with a very strong benchmark adjuvant. Taken together we have reported in this paper on a novel class of pH-degradable polymers that are highly efficient in formulating hydrophobic compounds. Exemplified for Amphotericin B, it dramatically reduces the cytotoxicity of this small molecule but retains its Toll like receptor agonist activity *in vitro* and holds excellent vaccine adjuvant properties in mouse models.

EXPERIMENTAL PROCEDURES

Synthesis of N-[2-[(tetrahydro-2H-pyran-2-yl)oxy]ethyl]-acrylamide (HEAmTHP)

Camphorsulfonic acid (1.630 g, 7.02 mmol) and N-(2-hydroxyethyl)acrylamide (7.5 mL, 70.2 mmol) were dissolved in 100 mL dry DCM. To this mixture 3,4-dihydro-2H-pyran (7.68 mL, 70.2 mmol) was added dropwise at 0°C. The reaction mixture was allowed to stir at RT under N_2. After 3h the reaction is quenched by addition of TEA. The mixture was concentrated *in vacuo*, dissolved in ethyl acetate and filtered. The filtrate was concentrated and purified by column chromatography (DCM/MeOH - 98:2 + 1% TEA) to give 11.9 g (85% yield) of a clear viscous oil. ^{1}H-NMR (300 MHz, DMSO-d6) δ ppm 1.38 - 1.52 (m, 4 H) 1.56 - 1.66 (m, 1 H) 1.66 - 1.84 (m, 1 H) 3.21 - 3.32 (m, 2 H) 3.36 - 3.47 (m, 2 H) 3.58 - 3.68 (m, 1 H) 3.73 (ddd, J=11.16, 7.86, 3.20 Hz, 1 H) 4.56 (t, J=3.58 Hz, 1 H) 5.50 - 5.62 (m, 1 H) 6.07 (dd, J=17.05, 2.35 Hz, 1 H) 6.25 (dd, J=17.05, 10.08 Hz, 1 H) 8.16 (br. s., 1 H). ^{13}C-NMR (75 MHz, DMSO-d6) δ ppm 164.66, 131.72, 125.03, 98.05, 65.41, 61.39, 38.71, 30.19, 24.99, 19.15. (ESI-MS) m/z = 200.1281 [M+H$^+$].

Determination of hydrolysis rate of acetal bearing monomers.

Monomer solutions were prepared at 5 mg/mL in 100 mM acetate buffer pH 5 and 100 mM phosphate buffer pH 7.4 in triplicate. A trace amount of hydroquinone monomethyl ether (200 ppm) was added to avoid polymerization. The solutions were stirred at 37°C. At regular time points samples are taken by diluting 20 µL of the hydrolysis solution into 180 µL 100 mM phosphate buffer pH 7.4 and stored at -18°C. Prior to injection the samples were diluted 50 times with eluent and analyzed by HPLC using water/acetonitrile 60:40 as eluent, with the flow rate set at 0.2 mL/min and detection at 207 nm. Assessment of the hydrolysis rate was done taking the ratio of molar concentrations of the compounds (equation 1) calculated from calibration curves for HEAmTHP and HEAm (**Figure S3**).

$$\%\, hydrolysis = \frac{[HEAm]}{([HEAm]+[HEAmTHP])} * 100 \qquad \text{eq. 1}$$

RAFT homopolymerization of HEAmTHP

pHEAmTHP$_{42}$ and pHEAmTHP$_{66}$ were synthesized following the same protocol with only altering the amount of PABTC and AIBN. As an example, the protocol for pHEAmTHP$_{42}$ is given here. A Schlenk tube was loaded with HEAm-THP (600 mg, 3 mmol), 2-(butylthiocarbonothioylthio)propanoic acid (PABTC) (14.35 mg, 0.06 mmol) and AIBN (1.97 mg, 0.012 mmol) and dissolved in dry DMF (2M). The mixture was degassed by five freeze-pump-thaw cylces and immersed in a pre-heated oil bath at 80°C under vigorous stirring. After 1h the reaction was quenched by cooling and exposure to air. The resulting polymer was isolated by repeated precipitations in ice-cold diethyl ether with acetone for re-dissolving the polymer. The precipitated polymer was dried under vacuum to give 300 mg yellow powder. Samples were taken before and after the polymerization and analysed by ^{1}H NMR to determine monomer conversion. Polydispersity of purified

polymer was analyzed by size exclusion chromatography (SEC). ^{1}H-NMR (300 MHz, DMSO-d6) δ ppm 1.25–2.55 (m, 9H), 3.34–3.47 (br.s, 2H), 3.48-3.68 (br.s, 2H), 3.72-3.85 (br.s, 1H), 3.85-4.0 (br.s, 1H), 4.5-4.7 (br.s, 1H).

Conditions for pHEAmTHP$_{66}$: HEAm-THP (600 mg, 3 mmol), 2-propanoic acid butyl trithiocarbonate (7.18 mg, 0.03 mmol) and AIBN (0.988 mg, 0.006 mmol).

Cloud point determination of HEAmTHP homopolymers

5 mg/mL polymer dispersions were made in PBS and cooled. The cooled solutions were filtered through a 0.450 µm filter before measurement to remove dust. The samples were analysed by DLS using a temperature trend going from 2°C to 20°C for the HEAmTHP homopolymers, temperature interval was set to 1°C with three repeated measurements for each temperature.

Determination of hydrolysis rate of HEAmTHP homopolymers

HEAmTHP hydrolysis mixtures were prepared by dissolving the polymer in cold buffer. The experiment is started by heating to 37°C while stirring. A 50 mM acetate buffer pH 5 + 1 M NaSCN and 50 mM phosphate buffer pH 7.4 + 1 M NaSCN were used as testing conditions. At regular time points a 4 mL sample was taken and dialysed against 0.1 % NH_4OH solution. All samples were dialysed 4 days during which the medium was frequently refreshed, followed by freeze drying. The freeze-dried samples were dissolved in deuterated methanol for NMR analysis, afterwards methanol was evaporated and 5 mg/mL sample solutions were made in 50 mM phosphate buffer pH 7.4 for turbidimetry measurement. Measurements were done by 3 repeated heating-cooling cycles and the average was used to plot the graphs.

RAFT homopolymerisation of pHEA macroCTA (pHEA)

Two pHEA macroCTAs with different chain length were synthesized following a similar protocol. Alterations in chain length were obtained by changing the ratio of HEA:PABTC from 100:1 to 150:1. As an example is the synthesis protocol for the ratio 100:1 is given below: To a Schlenk tube loaded with HEA (2.5 mL, 20.90 mmol) was added PABTC (49.82 mg, 0.209 mmol) and AIBN (6.86 mg, 0.0418 mmol) from a DMF stock solution. The mixture was diluted further with DMF to a total volume of 10.45 mL. The mixture was degassed by five freeze-pump-thaw cylces and immersed in a pre-heated oil bath at 70°C under vigorous stirring. After 1h the reaction was quenched by cooling and exposure to air. The resulting polymer was isolated by repeated precipitations in ice-cold diethyl ether with methanol for re-dissolving the polymer. The precipitated polymer was dried under vacuum to give 1.94 g of a yellow gel. Samples were taken before and after the polymerization and analysed by ^{1}H NMR to determine the monomer conversion. Polydispersity of purified

polymer was analyzed by SEC. ^{1}H-NMR (300 MHz, D_2O) δ ppm 1.50-2.20 (m, 2H), 2.24-2.64 (m, 1H), 3.67-3.89 (t, 2H), 4.00-4.32 (m, 2H).

RAFT block copolymerization of pHEA-HEAmTHP

Eight different block copolymers were made using the pHEA macroCTAs described above, of which four were prepared starting from $pHEA_{78}$macroCTA and four with $pHEA_{110}$ macroCTA. Variations in block lengths were achieved by altering the molar ratio HEAmTHP:pHEAmacroCTA. All polymerisations were conducted using the same experimental setup. The conditions for synthesis block copolymer with ratio 40:1 are given as an example: HEAmTHP (500 mg, 2.51 mmol) was weighted into a dry Schlenk tube with a stirring bar. To this $pHEA_{78}$ macroCTA (583.1 mg, 0.06275 mmol) and AIBN (2.06 mg, 0.0125 mmol) were added from a stock solutions in DMF. The mixture was diluted with DMF to a monomer concentration of 1 M. The mixture was degassed by five freeze-pump-thaw cycles and immersed in a pre-heated oil bath at 80°C under vigorous stirring. After 1h the reaction was quenched by cooling and exposure to air. The resulting polymer was isolated by repeated precipitations in ice-cold diethyl ether with methanol for re-dissolving the polymer. The precipitated polymer was dried under vacuum to give 820 mg of a yellow powder. Samples were taken before and after the polymerization and analysed by ^{1}H NMR to determine the monomer conversion. Polydispersity of purified polymer was analyzed by SEC. ^{1}H-NMR (300 MHz, MeOH-d4) δ ppm 1.14-2.16 (m, 11H), 2.18-2.43 (m, 1H), 3.04-3.31 (br.s, 2H), 3.35-3.48 (m, 2H), 3.48-3.67 (m, 3H), 3.68-3.85 (br.s, 1H), 3.88-4.11 (m, 2H), 4.45-4.64 (br.s, 1H), 4.65-4.85 (m, OH), 6.97-7.83 (br.s, NH).

Self-assembly behavior and temperature responsiveness of block copolymer nanoparticles

All experiments on the self-assembly and temperature responsiveness were evaluated at a polymer concentration of 5 mg/mL in either water or PBS and analysed by DLS. Polymer dispersions were made by dissolving the different block copolymers in cold solvent by sonication or vortex, subsequently all samples were filtered through a 0.450 μm filter to remove particles of dust. For measurements at 25°C the polymer dispersions were allowed to heat to room temperature and vortexed again. Temperature responsiveness measurements were performed using a temperature trend going from 2°C to 30°C with a temperature interval of 1°C and triplicate measurements at each temperature.

Determination of critical aggregation concentration (CAC) of pHEA-HEAmTHP block copolymers

Determination of the CAC was done according to previously described protocols[26,53] using pyrene as a fluorescent probe. pHEA-HEAmTHP stock solutions were prepared at 0.5 mg/mL in 100 mM phosphate buffer pH 7.4. From this a dilution series was made ranging from 0.5 mg/mL to 0.001 mg/mL. All samples (5 mL)

were cooled and 16.67 µL of a 36 µg/mL pyrene stock solution in acetone was added. The polymer dispersions were incubated overnight at 37°C to induce particle formation and to evaporate acetone, prior and after incubation they were intensively vortexed. The dilution series for each block copolymer were made in triplicate. Fluorescence excitation spectra were collected by fluorescence spectrophotometry. The CAC was quantified based on a change in excitation intensity ratio at 338 and 333 nm for a series of concentrations.

pH-dependent degradation of pHEA-HEAmTHP block copolymers

pH-dependent degradation was evaluated at pH values of 5 and 7.4. All measurements were performed at a polymer concentration of 5 mg/mL at 37°C by DLS analysis. Polymer dispersions were made in PBS or a 100 mM acetate buffer pH 5 and analyzed at regular time points.

Encapsulation of a hydrophobic fluorescent dye

1,4-Bis[1-cyano-2-(diphenylamino)phenyl)vinyl]benzene (DSB) was used a model compound. Encapsulation of the hydrophobic DSB in polymer nanoparticles was achieved using a solvent displacement technique. First, a 250 µg/mL DSB stock solution was made in acetone. Next, 1 mL of pHEA-HEAmTHP dispersions (10 mg/mL) were prepared in PBS. To these polymer dispersions 40 µL of the DSB stock solution was added to obtain a final DSB concentration of 10 µg/mL. The DSB loaded NP dispersions were left overnight to evaporate acetone. They were then filtered to remove excess dye. Control samples for only PBS or **P03** were prepared by a similar protocol.

In vitro cellular uptake studies

Cellular uptake was investigated using confocal microscopy. $pHEA_{78}$-$HEAmTHP_{53}$ block copolymers loaded with DSB (see above) were used as testing formulation. PBS and pHEA macroCTA were used as control and comparison, respectively. DC2.4 cells were plated out on Willco-Dish glass bottom dishes (30 000 cells, suspended in 200 µL of culture medium) and incubated overnight. Next, 10 µL of the DSB loaded $pHEA_{78}$-$HEAmTHP_{53}$ particle solution was added and incubated overnight. Cells were then fixed and stained with Hoechst and CTB-AF555. For these purposes culture medium was aspirated and cells were washed with PBS. Next, 200 µL of 4 % paraformaldehyde was added and allowed to fixate for 30 min. A staining solution was prepared by adding Hoechst (10 µL, of a 1 mg/mL stock in DMSO) and CTB-AF555 (5 µL of a 1 mg/mL stock in PBS) to a PBS buffer containing 1 % of BSA (2 mL). After aspiration and washing, 200 µL of this staining solution was added to the fixed cells and incubated for 30 minutes at 37°C. Finally, the samples were washed with 1 % BSA PBS buffer and stored at 4°C.

Amphotericin B encapsulation

Encapsulation method evaluation

pHEA$_{78}$-HEAmTHP$_{37}$ was used as model polymer to test encapsulation of AmpB via solvent displacement. Experiments were performed at polymer concentration of 1 mg/mL, 5 mg/mL and 10 mg/mL, for each concentration 3 ratios of AmpB to polymer were tested, namely (1/10, 1/2 and 1/1). The protocol for 1 mg/mL polymer concentration is given briefly. pHEA-HEAmTHP (1mg) and AmpB (0.1 mg, 0.5 mg or 1.0 mg) were dissolved in 100 µL DMSO to give a clear deep yellow solution. This was diluted with 900 µL PBS by dropwise addition while stirring. The resulting mixture was filtered through a 0.450 µm filter to remove excess AmpB. Quantification is done by diluting the formulation to a polymer concentration of 100 µg/mL in DMSO and analyzed by UV-Vis spectrometry. The amount of encapsulated AmpB was taken as the mean value for the concentrations calculated by the calibration curves at the three absorption maxima of AmpB (**Figure S14**). From the determined AmpB concentration, encapsulation efficiency (EE) and drug loading (DL) can be calculated. These parameters are defined by the formulas:

$$EE = \frac{conc\ AmpB\ (measured)}{conc\ AmpB\ (added)}\ x\ 100\%$$

$$DL = \frac{AmpB\ (measured)}{AmpB\ (measured) + polymer}\ x\ 100\%$$

Evaluation of AmpB encapsulation in different pHEA-HEAmTHP polymer nanoparticles

A similar protocol was used as described above using 10 mg/mL polymer and 1 mg/mL AmpB. In summary, pHEA-HEAmTHP polymers (10 mg) and AmpB (1 mg) were dissolved in 100 µL DMSO. The mixtures were diluted with 900 µL PBS under stirring followed by filtration through a 0.450 µm filter. All samples were prepared in triplicate. 10 µL sample was taken and diluted to 1 mL with DMSO for AmpB quantification by UV-Vis. One sample of each formulation was dialysed against 1 L H_2O, with regular changes of medium. After 48 h the dispersion was collected and freeze-dried. A small fraction of the obtained freeze-dried powder was dissolved in DMSO and analysed by UV-Vis for AmpB quantification. Encapsulation efficiency and drug loading were calculated. A 5 mg/mL dispersion was made in PBS and measured by DLS (**Figure S17**).

Preparation of AmpB-NP formulations

AmpB-NP formulations used for further testing were prepared for pHEA$_{78}$-HEAmTHP$_{37}$ (**P2**) and pHEA$_{110}$-HEAmTHP$_{47}$ (**P6**) using an optimized method. Polymer was dispersed in PBS at a concentration of 10 mg/mL.

To this AmpB was added dropwise under vigorous stirring from a 10 mg/mL stock solution is DMSO to have a 1:10 AmpB-polymer ratio. The dispersions were filtered through a 0.450 µm filter, dialysed against H_2O and freeze dried. The freeze dried AmpB-NPs were redispersed in PBS in a desired volume and the exact concentration was determined by UV-Vis spectroscopy.

In vitro cytotoxicity of AmpB NP formulations

AmpB NP stock solutions were prepared by dispersion of the freeze-dried sample in sterile PBS at a concentration of 20 mg/mL formulation followed by UV-Vis quantification. Based on this a dilution series was made by two-fold dilutions starting from 150 µM AmpB. Polymer control samples were prepared using the same dilution scheme starting from a 20 mg/mL stock solution in sterile PBS. The AmpB dilution series was made in DMSO with two-fold dilutions starting from 4.5 mM. RAW 264.7 macrophages were seeded in 96 well plates at a density of 300 000 cells/mL (120 µL per well) and incubated at 37°C overnight. 30 µL of sample (1 µL for AmpB dilutions in DMSO), PBS (negative control) or DMSO (positive control) were added and incubated for 24h followed by addition of 40 µL MTT reagent (1 mg/mL in PBS). After an incubation period of 2-3 h the formed formazan crystals were dissolved by addition of a 10% m/v SDS/0.01 M HCl solutions and incubated overnight. Quantification was done by measuring the absorbance at 590 nm using a microplate reader. Cell viability (%) can be defined as follows:

$$cell\ viability = \frac{Abs\ (sample) - Abs(+control)}{Abs(-control) - Abs(+control)}\ x\ 100\%$$

In vitro cell stimulation assay

AmpB NP stock solutions were made by dispersion of the freeze-dried sample in sterile PBS at a concentration of 20 mg/mL formulation followed by UV-Vis quantification. Based on this a dilution series was made by two-fold dilutions starting from 1 mM AmpB. Polymer control samples were made using the same dilution scheme starting from a 20 mg/mL stock solution in sterile PBS. The AmpB dilution series was made in DMSO with two-fold dilutions starting from 20 mM.

NF-kB/AP-1 activation assay was performed as recommended by the manufacturer (InvivoGen). RAW-Blue™ cell were seeded in 96 well plates at a density of 500 000 cells/mL (180 µL per well) and incubated at 37°C. Each well was pulsed with 20 µL sample or PBS (negative control on each plate) for the AmpB NP formulations and polymer control. AmpB dilutions in DMSO were tested by addition of 1 µL of sample or DMSO (control) and brought to a final volume of 200 µL by adding 19 µL PBS, 20 µL PBS was used as a negative control. After overnight incubation, the supernatant from each well was collected and probed for

secreted embryonic alkaline phosphatase (SEAP) using the QUANTI-Blue™ assay (InvivoGen). To 50 µL supernatant was added 150 µL QUANTI-Blue and incubated at 37°C. SEAP levels were determined by measuring optical density at 620 nm using a microplate reader. Activity was determined by the increase in optical density relative to the negative control.

In vivo evaluation

Mice

Specific pathogen-free, female BALB/c mice were obtained from Charles River Italy. The mice were housed under specific pathogen-free conditions in individually ventilated cages in a controlled 12h day-night cycle and given food and water ad libitum. All mice were 8 weeks old at the start of the experiments. The animal facility operates under the Flemish Government License Number LA1400536. All experiments were done under conditions specified by European law and authorized by the Institutional Ethical Committee on Experimental Animals.

Immunizations

Mice of 8 weeks were immunized subcutaneously with 20 µg antigen dissolved in PBS to a total volume of 100 µl. Depending on the group PBS, nanoparticle with or without AmpB-NPs or Sigma Adjuvant System (Sigma-Aldrich, St. Louis, USA) was added to the vaccine. Samples containing AmpB-NPs were made by dissolving the formulation at a 2 mg/mL AmpB concentration in PBS, this was diluted 1:1 with PSB (AmpB-NP) or with a 0.4 mg/mL SHe-KLH solution in PBS (Ag+AmpB-NP). Empty nanoparticle control samples were made by mixing a 20 mg/mL **P6** solution in PBS with a 0.4 mg/mL SHe-KLH solution in PBS (Ag+NP). Immunizations were performed two times at a 3-week interval. Blood samples were collected from the lateral tail vein once before immunization and two weeks after each immunization. First blood was left at 37°C for 30 min to clot. Thereafter, serum was collected by taking the supernatant from two consecutive centrifugations. The serum titers of SHe-peptide IgG were determined by peptide ELISA.

Infection of mice with RSV

Three weeks after the second immunization, the mice were sedated with isoflurane and infected intranasally with 10^6 PFU of HRSV A2. Five days after infection, the mice were sacrificed and whole lungs were collected and homogenized with a Tissue lyser II (Qiagen) in 1.0 ml HBSS containing 20% sucrose. The lung homogenates were cleared by centrifugation (1000 xg, 15 min, 4°C) and used to determine the viral titer by plaque assay on Vero cells.

Peptide ELISA

To determine SHe-specific IgG, IgG1 or IgG2a antibody titers in the sera off individual mice, a peptide ELISA was performed. First, the wells of a micotiter plates (type II F96 MaxiSorp,Nunc) were coated overnight at 37°C with 0.2 µg SHe peptide corresponding to the natural ectodomain of HRSV A2 (NKLCEYNVFHNKT-FELPRARVNT) in 100 µl of 50 mM sodium bicarbonate buffer (pH 9.7). After incubation, the plates were washed three times with PBS and blocked for 1h at room temperature with 200 µl of 1% BSA in PBS. After this blocking step, the plates were washed again 3 times. Series of threefold dilutions of the different mouse serum samples, starting with a 1/100 dilution, were loaded on the coated plates for 1h30 at room temperature. Next, horseradish peroxidase labelled antibodies directed against mouse isotype IgG, IgG1 or IgG2a (diluted 1/6000) (Southern Biotechnology Associates, Inc., Birmingham, AL, USA) in PBS + 1% BSA +0.05 % Tween 20 were added to detect the bound antibodies. After washing, the microtites plates were incubated for 5 min with TMB substrate (tet-ramethylbenzidine, Sigma-Aldrich). The reaction was stopped by adding an equal volume 1M H2SO4 and absorbance at 450 nm was measured.

Plaque assay

Fifty µl of serial three-fold dilutions of the lung homogenates were added to a monolayers of Vero cells in a 96-well plate. The Vero cells were cultured in serum free OptiMEM medium (Invitrogen) supplemented with penicillin and streptomycin. After 3h, the medium was removed from the Vero cells and 150 µl of growth medium containing 2% FCS and 0.6% avicel RC-851 (FMC Biopolymers) was added to the cells for 3 days at 37°C. After infection, the cells were washed twice with PBS and subsequently fixed in 2% paraformaldehyde during 30 min. The cells were washed twice with PBS, permeabilized with 0,1% Triton-X100 and blocked with PBS containing 1% BSA. To stain the viral plaques, a polyclonal goat anti-HRSV serum (AB1128, Chemicon International) (1/4,000) was added during 1h. After washing three times with 1% BSA in PBS, the wells were incubated with HRP-conjugated anti-goat IgG antibodies (SC2020, Santa Cruz) for 30 min. Non-binding antibodies were removed by four washing steps with PBS containing 1% BSA and 0.01% Triton X-100 and one wash with PBS. Finally, TrueBlue peroxidase substrate (KPL, Gaithersburg) was added to visualize the plaques. The plaques of three different dilutions were counted and for each dilution, the number of PFU per lung (1ml of lung homogenate) was calculated as the number of plaques present in a given dilution multiplied by the dilution factor, times 20 (20 = 1000 µl total supernatant volume/50 µl of supernatant used to infect the first well of dilution series). The number of PFU/lung was then calculated as the average number of PFU/lung calculated for the different dilutions.

ASSOCIATED CONTENT

Additional experimental data are included in supporting information.

ACKNOWLEDGEMENTS

B.L., L.L. and R.D.C. thank the IWT Flanders and Ghent University (BOF), respectively, for scholarships. B.G.D.G. acknowledges the FWO Flanders and the Flemish Liga Against Cancer for funding. L.N. thanks the FWO Flanders and the Alexander von Humboldt Foundation for a Feodor Lynen fellowship. LVH is a junior assistant and BS a post-doctoral assistant of the Ghent University department of Biomedical Molecular Biology. We also thank Olivier Stephan for kindly providing us with DSB. S.V.H. wants to thank Silke Verdonck for her contributions in the experimental work during her master thesis.

The authors declare no competing financial interest.

ABBREVIATIONS

AmpB, amphotericin B; RSV, respiratory syncytial virus; HEAm, 2-hydroxyethylacrylamide; DHP, 3,4-dihydro-2H-pyran; HEAmTHP, N-[2-[(tetrahydro-2H-pyran-2-yl)oxy]ethyl]-acrylamide; PBS, phosphate buffer saline; PABTC, 2-(butylthiocarbonothioylthio)propanoic acid; DP, degree of polymerization; HEA, 2-hydroxyethylacrylate; CAC, critical association concentration; Tcp, cloud point temperature; DSB, 1,4-bis[1-cyano-2-(diphenylamino)phenyl)vinyl]benzene; DC2.4, dendritic cell line; DMSO, dimethyl sulfoxide; AmpB-NP, AmpB nanoparticles; SHe, small hydrophobic extracellular protein of RSV; KLH, keyhole limpet hemocyanin; SAS, Sigma Adjuvant System; MPLA, monophosphoryl lipid A.

REFERENCES

(1) Gammon, J. M., Dold, N. M., Jewell, C. M. (2016) Improving the clinical impact of biomaterials in cancer immunotherapy. *Oncotarget 7*, 15421–43.

(2) Jeanbart, L., Swartz, M. A. (2015) Engineering opportunities in cancer immunotherapy. *Proc. Natl. Acad. Sci. U. S. A. 112*, 14467–72.

(3) Maisonneuve, C., Bertholet, S., Philpott, D. J., De Gregorio, E. (2014) Unleashing the potential of NOD- and Toll-like agonists as vaccine adjuvants. *Proc. Natl. Acad. Sci. 111*, 12294–12299.

(4) Iwasaki, A., Medzhitov, R. (2015) Control of adaptive immunity by the innate immune system. *Nat. Immunol. 16*, 343–353.

(5) Mancini, R. J., Stutts, L., Ryu, K. A., Tom, J. K., Esser-Kahn, A. P. (2014) Directing the immune system with chemical compounds. *ACS Chem. Biol. 9*, 1075–1085.

(6) Fox, C. B., Moutaftsi, M., Vergara, J., Desbien, A. L., Nana, G. I., Vedvick, T. S., Coler, R. N., Reed, S. G. (2013) TLR4 ligand formulation causes distinct effects on antigen-specific cell-mediated and humoral immune responses. *Vaccine 31*, 5848–5855.

(7) Nuhn, L., Vanparijs, N., De Beuckelaer, A., Lybaert, L., Verstraete, G., Deswarte, K., Lienenklaus, S., Shukla, N. M., Salyer, A. C. D., Lambrecht, B. N., et al. (2016) pH-degradable imidazoquinoline-ligated nanogels for lymph node-focused immune activation. *Proc. Natl. Acad. Sci. U. S. A. 113*, 8098–103.

(8) Hartmann, S., Nuhn, L., Palitzsch, B., Glaffig, M., Stergiou, N., Gerlitzki, B., Schmitt, E., Kunz, H., Zentel, R. (2015) CpG-loaded multifunctional cationic nanohydrogel particles as self-adjuvanting glycopeptide antitumor vaccines. *Adv. Healthc. Mater. 4*, 522–527.

(9) Wu, T. Y.-H., Singh, M., Miller, A. T., Gregorio, E. De, Doro, F., Oro, U. D., Skibinski, D. a. G., Mbow, M. L., Bufali, S., Herman, A. E., et al. (2014) Rational design of small molecules as vaccine adjuvants. *Sci. Transl. Med. 6*, 160–263.

(10) Tom, J. K., Dotsey, E. Y., Wong, H. Y., Stutts, L., Moore, T., Davies, D. H., Felgner, P. L., Esser-Kahn, A. P. (2015) Modulation of Innate Immune Responses via Covalently Linked TLR Agonists. *ACS Cent. Sci. 1*, 439–448.

(11) Kranz, L. M., Diken, M., Haas, H., Kreiter, S., Loquai, C., Reuter, K. C., Meng, M., Fritz, D., Vascotto, F., Hefesha, H., et al. (2016) Systemic RNA delivery to dendritic cells exploits antiviral defence for cancer immunotherapy. *Nature 534*, 396–401.

(12) Kasturi, S. P., Skountzou, I., Albrecht, R. A., Koutsonanos, D., Hua, T., Nakaya, H. I., Ravindran, R., Stewart, S., Alam, M., Kwissa, M., et al. (2011) Programming the magnitude and persistence of antibody responses with innate immunity. *Nature 470*, 543–7.

(13) Salyer, A. C. D., Caruso, G., Khetani, K. K., Fox, L. M., Malladi, S. S., David, S. A. (2016) Identification of adjuvantic activity of amphotericin B in a novel, multiplexed, poly-TLR/NLR high-throughput screen. *PLoS One 11*, 1–17.

(14) Torrado, J. J., Espada, R., Ballesteros, M. P., Torrado-Santiago, S. (2008) Amphotericin B Formulations and Drug Targeting. *J. Pharm. Sci. 97*, 2405–2425.

(15) Yu, B. ., Okano, T., Kataoka, K., Sardari, S., Kwon, G. . (1998) In vitro dissociation of antifungal efficacy and toxicity for amphotericin B-loaded poly(ethylene oxide)-block-poly(β-benzyl-l-aspartate) micelles. *J. Control. Release 56*, 285–291.

(16) Asthana, S., Jaiswal, A. K., Gupta, P. K., Dube, A., Chourasia, M. K. (2015) Th-1 biased immunomodulation and synergistic antileishmanial activity of stable cationic lipid–polymer hybrid nanoparticle: Biodistribution and toxicity assessment of encapsulated amphotericin B. *Eur. J. Pharm. Biopharm. 89*, 62–73.

(17) Sau, K., Mambula, S. S., Latz, E., Henneke, P., Golenbock, D. T., Levitz, S. M. (2003) The antifungal drug amphotericin B promotes inflammatory cytokine release by a toll-like receptor- and CD14-dependent mechanism. *J. Biol. Chem. 278*, 37561–37568.

(18) Irvine, D. J., Hanson, M. C., Rakhra, K., Tokatlian, T. (2015) Synthetic Nanoparticles for Vaccines and Immunotherapy. *Chem. Rev. 115*, 11109–11146.

(19) Bachmann, M. F., Jennings, G. T. (2010) Vaccine delivery: a matter of size, geometry, kinetics and molecular patterns. *Nat. Rev. Immunol. 10*, 787–96.

(20) Liu, H., Moynihan, K. D., Zheng, Y., Szeto, G. L., Li, A. V, Huang, B., Van Egeren, D. S., Park, C., Irvine, D. J. (2014) Structure-based programming of lymph-node targeting in molecular vaccines. *Nature 507*, 519–22.

(21) Lynn, G. M., Laga, R., Darrah, P. A., Ishizuka, A. S., Balaci, A. J., Dulcey, A. E., Pechar, M., Pola, R., Gerner, M. Y., Yamamoto, A., et al. (2015) In vivo characterization of the physicochemical properties of polymer-linked TLR agonists that enhance vaccine immunogenicity. *Nat. Biotechnol. 33*, 1201–10.

(22) Ilyinskii, P. O., Roy, C. J., O'Neil, C. P., Browning, E. A., Pittet, L. A., Altreuter, D. H., Alexis, F., Tonti, E., Shi, J., Basto, P.

et al. (2014) Adjuvant-carrying synthetic vaccine particles augment the immune response to encapsulated antigen and exhibit strong local immune activation without inducing systemic cytokine release. *Vaccine 32*, 2882–2895.

(23) Vanparijs, N., Nuhn, L., De Geest, B. G. (2017) Transiently thermoresponsive polymers and their applications in biomedicine. *Chem. Soc. Rev. 46*, 1193–1239.

(24) de Las Heras Alarcon, C., Pennadam, S., Alexander, C. (2005) Stimuli responsive polymers for biomedical applications. *Chem. Soc. Rev. 34*, 276–285.

(25) Binauld, S., Stenzel, M. H. (2013) Acid-degradable polymers for drug delivery: a decade of innovation. *Chem. Commun. (Camb). 49*, 2082–102.

(26) Louage, B., Zhang, Q., Vanparijs, N., Voorhaar, L., Vande Casteele, S., Shi, Y., Hennink, W. E., Van Bocxlaer, J., Hoogenboom, R., De Geest, B. G. (2015) Degradable Ketal-based block copolymer nanoparticles for anticancer drug delivery: A systematic evaluation. *Biomacromolecules 16*, 336–350.

(27) Jain, R., Standley, S. M., Fréchet, J. M. J. (2007) Synthesis and Degradation of pH-Sensitive Linear Poly (amidoamine) s. *Macromolecules 40*, 452–457.

(28) Heffernan, M. J., Murthy, N. (2005) Polyketal Nanoparticles: A New pH-Sensitive Biodegradable Drug Delivery Vehicle. *Bioconjug. Chem. 16*, 1340–1342.

(29) Murthy, N., Xu, M., Schuck, S., Kunisawa, J., Shastri, N., Fréchet, J. M. J. (2003) A macromolecular delivery vehicle for protein-based vaccines: acid-degradable protein-loaded microgels. *Proc. Natl. Acad. Sci. U. S. A. 100*, 4995–5000.

(30) Shenoi, R. A., Narayanannair, J. K., Hamilton, J. L., Lai, B. F. L., Horte, S., Kainthan, R. K., Varghese, J. P., Rajeev, K. G., Manoharan, M., Kizhakkedathu, J. N. (2012) Branched multifunctional polyether polyketals: Variation of ketal group structure enables unprecedented control over polymer degradation in solution and within cells. *J. Am. Chem. Soc. 134*, 14945–14957.

(31) Lingier, S., Nevejans, S., Espeel, P., De Wildeman, S., Du Prez, F. E. (2016) High molecular weight poly(cycloacetals) towards processable polymer materials. *Polymer (Guildf). 103*, 98–103.

(32) Zou, Y., Brooks, D. E., Kizhakkedathu, J. N. (2008) A Novel Functional Polymer with Tunable LCST. *Macromolecules 41*, 5393–5405.

(33) Vanparijs, N., De Coen, R., Laplace, D., Louage, B., Maji, S., Lybaert, L., Hoogenboom, R., De Geest, B. G. (2015) Transiently responsive protein-polymer conjugates via a “grafting-from” RAFT approach for intracellular co-delivery of proteins and immune-modulators. *Chem. Commun. (Camb). 51*, 13972–5.

(34) Wuts, P. G. M., Greene, T. W. (2006) Greene’s Protective Groups in Organic Synthesis 4th ed. John Wiley & Sons, Inc., Hoboken, NJ, USA.

(35) Klaikherd, A., Nagamani, C., Thayumanavan, S. (2009) Multi-Stimuli Sensitive Amphilic Block Copolymer Assemblies. *J. Am. Chem. Soc. 131*, 4830–4838.

(36) Gil, E. S., Hudson, S. M. (2004) Stimuli-reponsive polymers and their bioconjugates. *Prog. Polym. Sci. 29*, 1173–1222.

(37) Gibson, M. I., O’Reilly, R. K. (2013) To aggregate, or not to aggregate? considerations in the design and application of polymeric thermally-responsive nanoparticles. *Chem. Soc. Rev. 42*, 7204–7213.

(38) De Coen, R., Vanparijs, N., Risseeuw, M. D. P., Lybaert, L., Louage, B., De Koker, S., Kumar, V., Grooten, J., Taylor, L., Ayres, N., V et al. (2016) pH-Degradable Mannosylated Nanogels for Dendritic Cell Targeting. *Biomacromolecules 17*, 2479–2488.

(39) Fernandes Stefanello, T., Szarpak-Jankowska, A., Appaix, F., Louage, B., Hamard, L., De Geest, B. G., van der Sanden, B., Nakamura, C. V., Auzély-Velty, R. (2014) Thermoresponsive hyaluronic acid nanogels as hydrophobic drug carrier to macrophages. *Acta Biomater. 10*, 4750–4758.

(40) Palacios, D. S., Dailey, I., Siebert, D. M., Wilcock, B. C., Burke, M. D. (2011) Synthesis-enabled functional group deletions reveal key underpinnings of amphotericin B ion channel and antifungal activities. *Proc. Natl. Acad. Sci. U. S. A. 108*, 6733–6738.

(41) Mehta, R. T., Mehta, K., Lopez-Berestein, G., Juliano, R. L. (1985) Effect of liposomal amphotericin B on murine macrophages and lymphocytes. *Infect. Immun. 47*, 429–433.

(42) Borowski, E., Cybulska, B. (1967) Potassiumless Death of Saccharomyces cerevisiae Cells treated with N-Succinyl Perimycin and the Reversal of Fungicidal Action of the Antibiotic by Potassium Ions. *Nature 213*, 1034–1035.

(43) Endo, M. M., Cioffi, A. G., Burke, M. D. (2016) Our Path to Less Toxic Amphotericins. *Synlett 27*, 337–354.

(44) Volmer, A. A., Szpilman, A. M., Carreira, E. M. (2010) Synthesis and biological evaluation of amphotericin B derivatives. *Nat. Prod. Rep. 27*, 1329.

(45) Barwicz, J., Christian, S., Gruda, I. (1992) Effects of the aggregation state of amphotericin B on its toxicity to mice. *Antimicrob. Agents Chemother. 36*, 2310–2315.

(46) Iwasaki, A., Medzhitov, R. (2004) Toll-like receptor control of the adaptive immune responses. *Nat. Immunol. 5*, 987–95.

(47) Francica, J. R., Lynn, G. M., Laga, R., Joyce, M. G., Ruckwardt, T. J., Morabito, K. M., Chen, M., Chaudhuri, R., Zhang, B., Sastry, M., et al. (2016) Thermoresponsive Polymer Nanoparticles Co-deliver RSV F Trimers with a TLR-7/8 Adjuvant. *Bioconjug. Chem. 27*, 2372–2385.

(48) Stein, R. T., Bont, L. J., Zar, H., Polack, F. P., Park, C., Claxton, A., Borok, G., Butylkova, Y., Wegzyn, C. (2017) Respiratory syncytial virus hospitalization and mortality: Systematic review and meta-analysis. *Pediatr. Pulmonol. 52*, 556–569.

(49) Lotz, M. T., Moore, M. L., Peebles, R. S. (2013) Respiratory Syncytial Virus and Reactive Airway Disease, in *Curr Top Microbiol Immunol*, pp 105–118.

(50) Schepens, B., Sedeyn, K., Vande Ginste, L., De Baets, S., Schotsaert, M., Roose, K., Houspie, L., Van Ranst, M., Gilbert, B., Van Rooijen, N., et al. (2014) Protection and mechanism of action of a novel human respiratory syncytial virus vaccine candidate based on the extracellular domain of small hydrophobic protein. *EMBO Mol Med 6*, 1436–1454.

(51) Ferguson, C. J., Hughes, R. J., Nguyen, D., Pham, B. T. T., Gilbert, R. G., Serelis, A. K., Such, C. H., Hawkett, B. S. (2005) Ab Initio Emulsion Polymerization by RAFT-Controlled Self-Assembly. *Macromolecules 38*, 2191–2204.

(52) Maurin, M., Vurth, L., Vial, J.-C., Baldeck, P., Marder, S. R., Sanden, B. Van der, Stephan, O. (2009) Fluorescent Pluronic nanodots for in vivo two-photon imaging. *Nanotechnology 20*, 235102.

(53) Kalyanasundaram, K., Thomas, J. K. (1977) Environmental effects on vibronic band intensities in pyrene monomer fluorescence and their application in studies of micellar systems. *J. Am. Chem. Soc. 99*, 2039–2044.

TOC